Sains Malaysiana 51(3)(2022): 657-677
http://doi.org/10.17576/jsm-2022-5103-03

Curie-point Depths, Geothermal Gradients and Sub-Surface Heat Flow Estimation from Spectral Analysis of High-Resolution Aeromagnetic Data over Gongola Basin and Its Environs, Northeastern Nigeria

(Kedalaman Titik Curie, Kecerunan Geoterma dan Anggaran Aliran Haba Sub-Permukaan daripada Analisis Spektrum Data Aeromagnetik Resolusi Tinggi di Lembangan Gongola dan Sekitarnya, Timur Laut Nigeria)

ABUBAKAR YUSUF[1,2], LIM HWEE SAN[1,*] & ISMAIL AHMAD ABIR[1]

[1]*Exploration Geophysics Section, School of Physics, Universiti Sains Malaysia, 11800 Penang, Malaysia*
[2]*Department of Geology, Faculty of Science, Gombe State University, P.M.B. 0127, Gombe, Nigeria*

Received: 20 March 2021/Accepted: 31 July 2021

ABSTRACT

Geothermal energy resources have been established globally to be among the sustainable and environmentally harmless means of energy generation. Curie-point depths (CPD), temperature gradients, and heat flow data over the study area were computed using a spectral analysis method in order to have a preliminary view of the geothermal implications (prospect) of the current area. Aeromagnetic data acquired by the Nigerian Geological Survey Agency (NGSA) in the year 2009 was used for the research. The results showed the minimum, maximum, and the average CPD values as 8.18 km, 31.48 km, and 13.0 km, respectively. The minimum, maximum and average thermal gradients obtained were 18.42 °C/km, 70.91 °C/km, and 50.2 °C/km, respectively. The heat flow data obtained ranged from 33.15 mW/m^2 to 177.28 mW/m^2, with an average value of 110.65 mW/m^2. Locations depicting shallow CPDs anomalies (Alkaleri, Darazo, Dukku, Misau, Wuyo, Deba, and Tula), also showed conformity with high heat flow areas. As such, they are regarded as areas of promising geothermal prospects and are recommended for further detailed investigation. Locations depicting a high magnetic susceptibility contrast from a generated analytic signal map, as well as high temperature gradients, high heat flow, and shallow CPDs are attributed to crustal thinning along the sedimentary basin and magmatic intrusions along basement areas, respectively. The magnetic depth to the basement calculated for the study area using the source parameter imaging (SPI) method ranges from 0.610 km to 3.055 km. The present study has provided an insight on preliminary information, regarding new areas of possible geothermal prospects for further detailed investigation.

Keywords: Aeromagnetic; Curie-point depth; heat flow; spectral analysis; temperature gradients

ABSTRAK

Sumber tenaga geoterma telah ditubuhkan secara global untuk menjadi antara kaedah penjanaan tenaga yang mampan dan tidak berbahaya kepada alam sekitar. Kedalaman titik Curie (CPD), kecerunan suhu dan data aliran haba ke atas kawasan kajian telah dihitung menggunakan kaedah analisis spektrum untuk mendapatkan pandangan awal tentang implikasi (prospek) geoterma bagi kawasan semasa. Data aeromagnet yang diperoleh oleh Agensi Kajian Geologi Nigeria (NGSA) pada tahun 2009 digunakan untuk penyelidikan. Keputusan menunjukkan nilai CPD minimum, maksimum dan purata masing-masing 8.18 km, 31.48 km dan 13.0 km. Kecerunan terma minimum, maksimum dan purata yang diperoleh ialah 18.42 °C/km, 70.91 °C/km dan 50.2 °C/km, masing-masing. Data aliran haba yang diperoleh adalah antara 33.15 mW/m2 hingga 177.28 mW/m2, dengan nilai purata 110.65 mW/m2. Lokasi yang menggambarkan anomali CPD cetek (Alkaleri, Darazo, Dukku, Misau, Wuyo, Deba dan Tula), juga menunjukkan pematuhan dengan kawasan aliran haba yang tinggi. Oleh itu, ia dianggap sebagai kawasan prospek geoterma yang menjanjikan dan disyorkan untuk kajian terperinci lanjut. Lokasi yang menggambarkan kontras kerentanan magnet yang tinggi daripada peta isyarat analitik yang dijana, serta kecerunan suhu tinggi, aliran haba yang tinggi dan CPD cetek dikaitkan dengan penipisan kerak di sepanjang lembangan sedimen dan pencerobohan magmatik di sepanjang kawasan bawah tanah.

Kedalaman magnet ke ruang bawah tanah yang dihitung untuk kawasan kajian menggunakan kaedah pengimejan parameter sumber (SPI) berjulat dari 0.610 km hingga 3.055 km. Kajian ini telah memberikan gambaran tentang maklumat awal, mengenai kawasan baharu prospek geoterma untuk kajian terperinci lanjut.

Kata kunci: Aeromagnetik; aliran haba; analisis spektrum; kecerunan suhu; kedalaman titik Curie

Introduction

Recently, geothermal energy has continued to gain attention in the global community as an alternative to environmentally harmful fossil fuels (Baioumy et al. 2014). In many countries, geothermal energy currently contributes to a substantial percentage of their energy generation. These include countries like Indonesia, Germany, France, Italy, and the United States of America, among others (Guo & Wang 2012).

However, despite several attempts by different geoscientists to study geothermal contents of different parts of the world using different scientific approaches (Abraham et al. 2019; Billim et al. 2015; Correa et al. 2016; Gailer et al. 2016; Mono et al. 2018; Obande et al. 2014; Saada 2016; Wang & Li 2018), some information regarding the crustal temperature contents of certain regions are not thoroughly understood. There were two main approaches to these studies: the first involves a direct approach in studying the shallower parts of the crust using bottom hole temperature measurements from drilled holes within crustal regions (Mohamed et al. 2015). The indirect approach uses potential field data to study the earth's crustal heat sources. The bottom hole temperature measurement approach is limited because it shows information that is localized and does not give a broader view of the necessary crustal temperature information. In contrast, the method that involves the use of geophysical data (magnetic, gravity) yields a better result that is broader and has extensive coverage (Saibi et al. 2015). Another limitation/constraint of the application of the direct method is that not all regions of the earth's crust are penetrated by drill holes; as such, areas without the boreholes cannot be properly understood in terms of their crustal heat information potential using this method.

The study area is among the crustal regions with minimal information on its crustal temperature endowments, and it is found in the Northern Benue trough of the northeastern geological terrain of Nigeria (Figure 1(a)). The area is bounded between 9° 30′ N to 11° 30′ N and 10° 00′E to 12° 00′E and occupies an area of 49,284 km^2 (Figure 1(b)). These aspects of the crust cannot be extensively studied by applying and relying on the bottom hole temperature measurement approach for the purpose of understanding its crustal heat contents for geothermal prospecting; this is because the approach does not guarantee a sufficient amount of drilled holes, and even where enough holes are present, extensive evaluations of the crust's geothermal potential cannot be performed. Hence, this study employed the use of new high-resolution aeromagnetic data by applying the spectral analysis method for estimating the CPD, temperature gradient, and the heat flow data. The use of airborne magnetic data for this study is advantageous in the sense that it provides wide coverage of a regional study; however, these data also have a depth clarity problem that is associated with survey dimensions as well as uncertainty that arises from the geological complications of an area (Saibi et al. 2015). The CPD is the depth at which ferromagnetic minerals of a rock transform to a paramagnetic form when it reached a certain temperature within the crust; it is also considered to be the depth to basal parts of magnetic sources of anomalies showed from a calculated energy spectrum (Lowrie 2007; Nagata 1961).

Several geophysical studies using airborne magnetic data have been conducted in the Benue trough; this includes the work of Ajayi and Ajakaiye (1981), who focused on determining the origin of the Benue valley itself. The study provided an insight on the presence of a 40 km rift structure that lies beneath the sedimentary cover there. Osazuwa et al. (1981) used gravity data to study the Benue trough. Their results showed the presence of a wide negative gravity anomaly that is typical of a depression (valley) filled with sediments. The study further showed areas with mantle upliftments that ranged from 2-5 km in addition to show other areas of crustal thinning.

Another geothermal occurrence evaluation study focusing on the geological manifestation was conducted by Abdullahi et al. (2014). The study showed the presence of thermal springs and the volcanic plug distribution around the Gongola basin. Moreover, Musa (2015) also conducted research on the distribution of mud volcanoes within the Gongola basin, with several concentrated around the Kaltungo and Billiri areas. Additionally,

the Nigerian Geological Survey Agency (NGSA 2009) conducted geological mapping of some regions in Nigeria in the year 2009; the report's maps showed the distribution of volcanic plugs within the Gongola basin. The presence of volcanic rocks in an area can be attributed to geothermal occurrences (Baioumy et al. 2014).

Furthermore, among the few attempts made to provide information on crustal heat in this region through the direct approach is the work of Kurowska and Schoenich (2010). This study provided some crustal heat information using temperature measurements from the few boreholes available in the area; however, their results did not provide the necessary extensive coverage because there were not enough boreholes to be used for a detailed study. Moreover, even when bore holes were available, they were limited by depth constraints, thereby only showing localized information. This highlights the need to use an indirect method (spectral analysis of aeromagnetic data) in showing information from deeper parts of the crust with broader coverage.

Currently, the few studies performed within this region have only concentrated on addressing the origin and structural configuration aspects. In addition to the few attempts to use either borehole temperature data or geological data to understand the thermal structure of this region, the present study obtains the missing crustal temperature information existing in this region using aeromagnetic data, which is more efficient. This research will be instrumental in showing the geothermal potentials of this area using the Curie-point depth (CPD) estimation by spectral analysis approach provided by Okubo et al. (1985) and Tanaka et al. (1999).

The aim of this research was to determine the preliminary geothermal potentials of this region. Thus, it was achieved via a number of objectives that include: estimation for CPD, temperature gradient, sub-surface heat flow, generation of horizontal gradient and analytic signal variation maps of the area, as well as the generation of a magnetic inversion to show the magnetized basement and compare its depth with depths from CPD.

As mentioned previously, the study area, set within the Northeastern terrain of Nigeria, covers the entire Gongola basin as well as some of the surrounding crystalline Precambrian basement and volcanic rocks adjoining it (Figure 1(a)). The rocks outcropping in the study area can be grouped into three main groups: Cretaceous sedimentary rocks of the Gongola basin, Precambrian basement rocks, and volcanic plugs that penetrated the pre-existing basement as well as the sedimentary succession (Musa 2015).

The stratigraphic succession of the Gongola basin of the Upper Benue trough was discussed by many authors (Abubakar 2006; Hamidu 2012; Nwajide 2013; Obaje 2009; Tukur et al. 2015). This succession commences with the deposition of Bima Formation, which overlies the Precambrian rocks unconformably. The Bima Formation, which is believed to have been deposited under a continental setting, comprises coarse to medium grained sandstones that are intercalated with clays, mudstones and shales (Abubakar 2006). The next lithologic (rock) unit overlying the Bima Formation is the Yolde Formation; this rock unit marked the beginning of a marine intrusion into the Benue trough. The Yolde Formation was deposited during a transitional period from continental to marine conditions and it is composed of sandstone, clay stone, and shales (Abubakar 2006). Moreover, overlying the Yolde Formation is the Pindiga Formation, which represents the full intrusion of marine conditions into the sub-basin during the Turonian age. The composition of this rock unit includes shales (carbonaceous) intercalated with limestone and minor sandstone (Nwajide 2013). This formation is entirely marine.

There was a period when folding and other deformational activities affected the entire Benue trough and resulted in the deformations seen on many rock units pre-dating it (Nwajide 2013). However, Post-Santonian rock units also exist in the Benue trough; these are the Gombe Formation (Continental) and Keri-Keri Formations (Continental). The deposition of the last two rock units shows the re-intrusion (return) of continental conditions in the Gongola basin (Obaje 2009).

The Precambrian basement rocks surrounding the Gongola basin to the west include older granitic rocks that were believed to have been formed from metamorphism of pre-existing sediments, thereby leading to the generation of migmatites and gneissic rocks (Obaje 2009). Other rocks outcropping in the area are medium to coarse grained biotite and biotite hornblende granites, charnokytes and Charnokytic rocks, ignimbrites, and banded gneisses (Figure 1(b)). Gongola basin is further surrounded to the east by the Hawal massifs and Biu Tartiary volcanics, by the exposures of Lunguda basalts towards the south eastern portion of the study area, and the porphyritic granites and biotite granites that form part of the Kaltungo Inlier around the Billiri to Kaltungo areas (Figure 1(b), below). The gneisses and migmatites were penetrated by the granites and their associated types during the major thermo tectonic events of Pan-African times (Abdullahi et al. 2019).

The foremost structural orientations in the basement terrain have NW-SE, E-W, NE-SW, and N-S patterns (Abdullahi et al. 2019). Some of these trends correspond to the orientation of the Benue trough, which shows that the pattern of the rift was prominently controlled by the pre-existing structural features.

Geological indicators of some geothermal occurrences reported within the Gongola basin area (Figure 1(b)) include the area's two main warm springs; these are referred to as Wikki warm spring, found within Yankari Game reserve and the Ruwan-Zafi warm spring, found near the Lafia Lamurde area near Numan town (Abdullahi et al. 2014; Kurowska & Schoenich 2010). Other indicators of geothermal occurrences include the numerous mud volcanoes found around the Billiri-Kaltungo area (Musa 2015) as well as the distribution of numerous volcanic plugs around Kaltungo, in addition to the outcrops of Lunguda and Biu basalts in the study area (NGSA 2009).

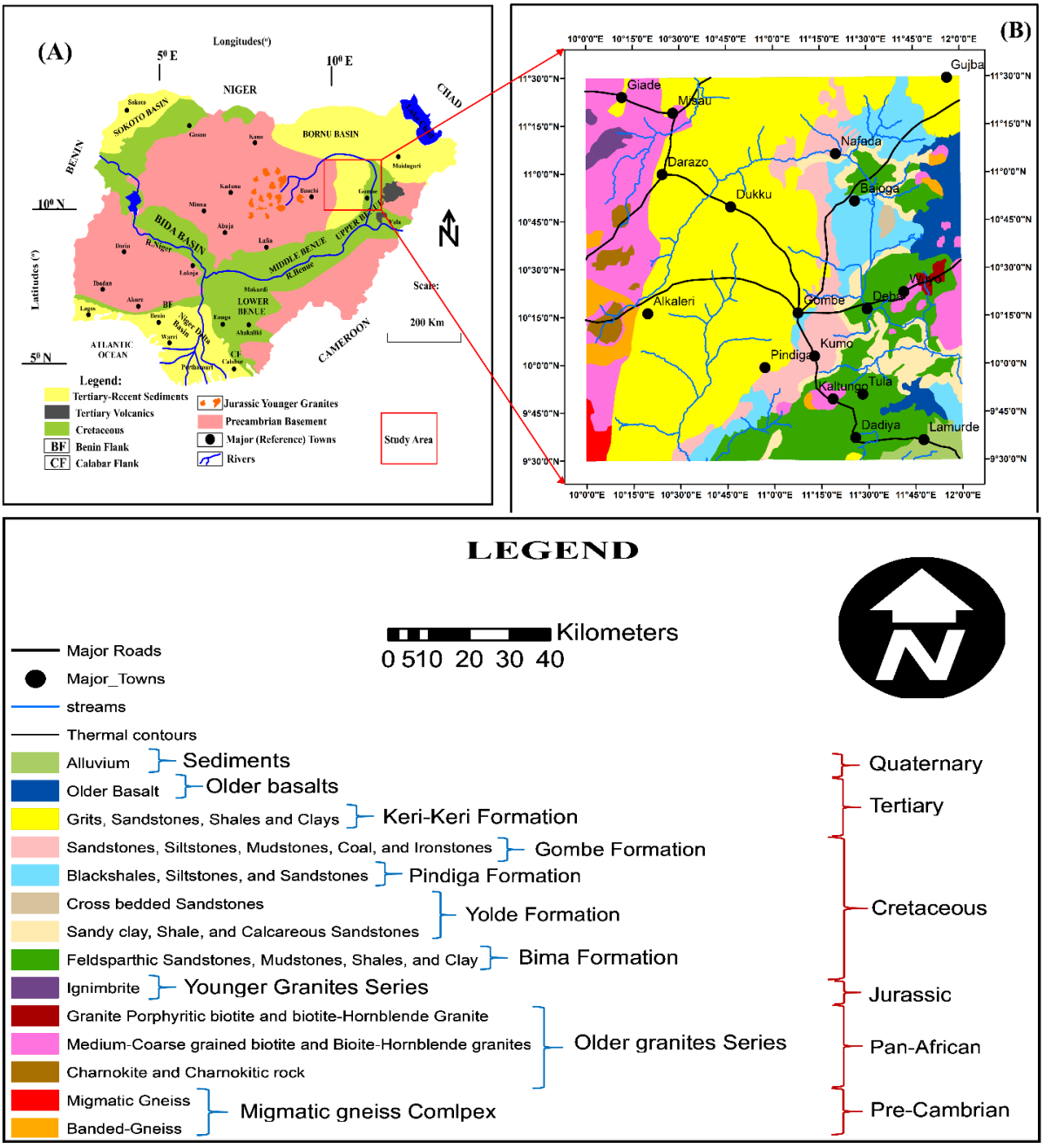

FIGURE 1. a) Geological map of Nigeria showing the position of the study area, and b) enlarged view of the geological map of the study area showing the rock distribution in the study area (Modified from NGSA 2009; Obaje 2009; Musa 2015)

Data and Methods

The aeromagnetic data used for this research was purchased from the Nigeria Geological Survey Agency (NGSA). This dataset is part of the newly acquired high-resolution aeromagnetic data that was acquired by Fugro - Aero Services Ltd within the years of 2004-2009, and it was acquired on behalf of the NGSA with the purpose of enhancing the research and development of Nigeria's energy and mineral sectors. The data was acquired at a spacing interval of 500 m, a terrain clearance of 80 m, a flight direction of NW-SE, tie-line spacing of 2 km, and a tie-line direction of NE-SW.

The acquired data was subjected to diurnal variation correction and an international geomagnetic reference field (IGRF) correction by the company that acquired it in 2010. A total of 16 aeromagnetic sheets were merged to form a composite grid that constituted the study area. These sheets include: Misau (107), Awiam (108), Nafada (109), Mutwe (110), Ganjuwa (129), Dukku (130), Bajoga (131), Gulani (132), Alkaleri (150), Akko (151), Gombe (152), Wuyo (153), Yuli (171), Futuk (172), Kaltungo (173), and Guyuk (174).

A total of 33000 nT, being the regional magnetic field components over Nigeria, was deducted from the acquired data by the processing company (Fugro - Aero-services) for the purpose of easy processing/presentation of the data. This component (factor) was added to the merged data to obtain the earth's total magnetic field measurements at every measurement point of the study area. Hence, the total magnetic field intensity (TMI) map of the area (Figure 2(a)) was created using a grid interval of 100 m. This fulfilled the 1/3 to 1/5 of the flight line interval requirements recommended by Dentith (2011). Considering the fact that the current study area is located in a low latitude zone. Therefore, they have non-centralized magnetic anomalies over their causative bodies, which is due to the bipolar nature of the earth's magnetic field (Adepelumi & Falade 2017; Stacey 1977). Hence, the (TMI) grid was subjected to reduction to equator (RTE) correction. RTE provides more reliable results compared to the reduction to pole (RTP) processing in low latitude areas (Jain 1988). Hence. The total magnetic field is reduced to the magnetic equator (RTE-TMI) map (Figure 2(b)) was produced. The RTE filter aids in re-positioning the anomalies over their sources. An inclination of -1.82° and a corresponding declination of -0.63° were used for the RTE correction.

The (RTE-TMI) grid was subjected to regional - residual separation using polynomial fitting method. The process results in the generation of two separate maps showing the earth's regional magnetic field components (Figure 3(a)) and the residual magnetic field of the study area (Figure 3(b)).

The residual map of the area, generated from applying polynomial fitting means of regional-residual separation, was filtered to a 15 km depth to eliminate shallow sources and enhance deep seated sources of residual anomalies. The residual map was later gridded into 49 overlapping grids, with each grid cell having a ½° by ½° dimension. This was performed so that each grid cell (Block) was overlapped by the succeeding grid by approximately 50% of its total grid surface area (Figure 4(a)). The central position of each grid cell is represented by a squared block, with each having a number denoting the block number. The upward continuation filter was used to suppress anomalies that were from shallow geological sources (bodies), and enhanced features from deeper sources usually considered to be from a greater depth; these features were characterized by long wavelength and low frequencies. This filter was used to compare the field that continued upward to a higher elevation level with that measured at the acquisition level.

Among the several procedures of determining the earth's crustal temperature is the CPD computation method using airborne magnetic data (Abdel Zaher et al. 2017; Aboud et al. 2011; Bello et al. 2017; Elbarbary et al. 2018; Maden 2010; Mono et al. 2018; Okubo et al. 1985; Saada 2016; Saleh et al. 2013). The CPD is the depth at which ferromagnesian minerals within the earth's crust lose their magnetism as a result of their transformation to a paramagnetic form. This transformation occurred due to the fact that the heat energy attained is adequate to retain the random orientation of magnetic moments of the iron-rich (dominant) minerals (Dunlop & Ozdemir 2001). A correlation exists between the CPD and the temperature of the earth's crust (Mono et al. 2018; Okubo et al. 1985). The CPD values over the study area were computed using the Centroid method that was earlier used by El Barbary et al. (2018), Okubo et al. (1985) and Tanaka et al. (1999). According to Okubo et al. (1985), and Tanaka et al. (1999), the depth to the central part of a source of magnetic anomaly (Z_0), and the depth to the top of magnetic source (Z_t), can be estimated from the slope of the radially averaged power spectrum plotted against its wave number (K). The central depth (Z_0), was obtained by using the slope of the low wavenumber part of the spectrum. The depth to top boundary of the magnetic source (Z_t), was computed from the slope of the high wave-number part of the spectrum.

Moreover, according to Tanaka et al. (1999), the source of the magnetic anomaly's layer extends infinitely in all horizontal directions. Therefore, it was assumed that

the depth to the top of the magnetic source is smaller than the horizontal scale of the magnetic source. Hence, the magnetization $M(_{x,y})$, takes a random function of x, and y. then, Blakely (1995) provided the power-density spectra of a total magnetic field to be given as;

$$\Phi_{\Delta T}: \Phi_{\Delta T}(k_x, k_y) = \Phi_m(k_x, k_y) \times F\left(k_x, k_y\right) \quad (1a)$$

But, $F(k_x, k_y) = 4\pi^2 (C_m^2) |\Theta_m|^2 |\Theta_f|^2 e^{-2|k|Z_t} \ (1^{-|k|(Z_b - Z_t)})^2$ (1b)

where $\Phi_{\Delta T}$ stands for the magnetization power-density spectra; C_m stands for the proportionality constant; Θ_m, and Θ_f represents factors for the direction of magnetization and direction of geomagnetic field, respectively. The equation can thus be simplified by noting that all terms except $|\Theta_m|^2$ and $|\Theta_f^2$ are radially symmetric. Furthermore, the radial average of Θ_m, and Θ_f are constants. If $M(_{x,y})$ is completely random and uncorrelated, then, $\Phi_m(k_x, k_y)$ is a constant, the radial average of $\Phi_{\Delta T}$ is then expressed as;

$$\Phi_{\Delta T}(|k|) = A e^{-2|k|Z_t} \ (1^{-|k|(Z_b - Z_t)})^2 \quad (2)$$

where A is a constant and k is the wave-number. For wavelength that is less than about twice the thickness of the layer, (2) can be expressed as;

$$In\left[\Phi_{\Delta T}(|k|)^{\frac{1}{2}}\right] = InB - |K|Z_t \quad (3)$$

where B is a constant. The top most boundary of the source of magnetic anomaly (Z_t) can be estimated by fitting a straight line through the second-longest segment of the radially average power spectrum $In\left[\Phi_{\Delta T}(|k|)^{\frac{1}{2}}\right]$.
Now, (2) can be re-expressed as;

$$\Phi_{\Delta T}(|k|)^{\frac{1}{2}} = Ce^{-|k|Z_o}(e^{-|k|(Z_t - Z_o)} - e^{-|k|(Z_b - Z_o)}) \quad (4)$$

where C is a constant. At long wavelengths, (4) can be re-expressed as;

$$\Phi_{\Delta T}(|k|)^{\frac{1}{2}} = Ce^{-|k|Z_o}\left(e^{-|k|(-d)} - e^{-|k|(d)}\right) = Ce^{-|k|Z_o} 2|k|d \quad (5)$$

where $2d$, represents the thickness of the source of magnetic anomaly. Now, (5), can be re-written as;

$$In\left\{\left[\Phi_{\Delta T}(|k|)^{\frac{1}{2}}\right]/|k|\right\} = InD - |k|Z_o \quad (6)$$

where D is a constant. Now, when a straight line is fitted through a segment of the radially average power spectrum with a longest wave-length, $In\left\{\left[\Phi_{\Delta T}(|k|)^{\frac{1}{2}}\right]/|k|\right\}$ Z_o can then be computed. Finally, the depth to the bottom part of the source of magnetic anomaly (which is the assumed CPD) can be calculated by using this relation;

$Z_b = 2Z_o - Z_t$ (7) (Okubo et al. 1985; Tanaka et al. 1999)

The graphs of the log of spectral energies for different spectral blocks were obtained by using the Geosoft software and a slope plot program mounted on MATLAB software. Each of the 49 spectral plots generated were first imported into a slope plot program (using MATLAB version-2018) to calculate different depths (Zt, and Z_0) from the different areas of interest of the spectral curve, as shown in (3) and (6) above and Figure 4(b) and 4(c). Thus, the CPD values for each of the blocks in Figure 4(a) was calculated using (7) by Okubo et al. 1985 and Tanaka et al. (1999), and the calculated results presented in Table 1. The CPD values generated were then contoured using the latitude and longitude values for the central points of each block against its CPD.

The temperature gradient and heat flow values were computed for the research area using Fourier's law as expressed in Elbarbary et al. (2018). The assumption in the equation was that the temperature variation trend (∂t) was upright (vertical) and that its gradients ($\frac{\partial t}{\partial Z}$) were constant. Then, the Curie temperature (θ) was related to the CPD (Z_b) and the thermal gradient ($\frac{\partial t}{\partial Z}$) in (8) and (9) presented by Okubo et al. (1985) and Elbarbary et al. (2018) as shown herewith:

$$\frac{\partial t}{\partial Z} = \frac{\theta}{Z_b} \quad (8)$$

$$Q = \lambda\left(\frac{\theta}{Z_b}\right) \quad (9)$$

where Q is the quantity of heat flow, and λ is the average thermal conductivity.

The θ of a magnetite, which is approximately 580 °C, was used for the computation of the temperature gradient. The average thermal conductivity for the studied igneous and sedimentary rocks were 2.5 W m^{-1} $^{\circ}C^{-1}$ and 1.80 W m^{-1} $^{\circ}C^{-1}$, respectively (Manea & Manea 2011; Mono et al. 2018; Onuoha & Ekine 1999; Stacey 1977).

The measure of the variation of Earth's magnetic field with respect to both x and y directions is termed the horizontal gradient estimation (Cordell & Grauch 1985; Verduzco et al. 2004). The magnitude of horizontal gradients for this area was computed by applying the

horizontal gradient filter to the residual grid (data) of the area using the MAGMAP tool of the Oasis montaj software. This filter can show the subsurface linear structural pattern of a given area. Linear features such as contact locations, faults, joints, and fractures are easily mapped using this filter (Cordell & Grauch 1985). To view the distribution of the mapped lineaments with respect to areas of high geothermal heat flow, an overlay of the mapped lineaments on the heat flow map was created (Figure 5(a)).

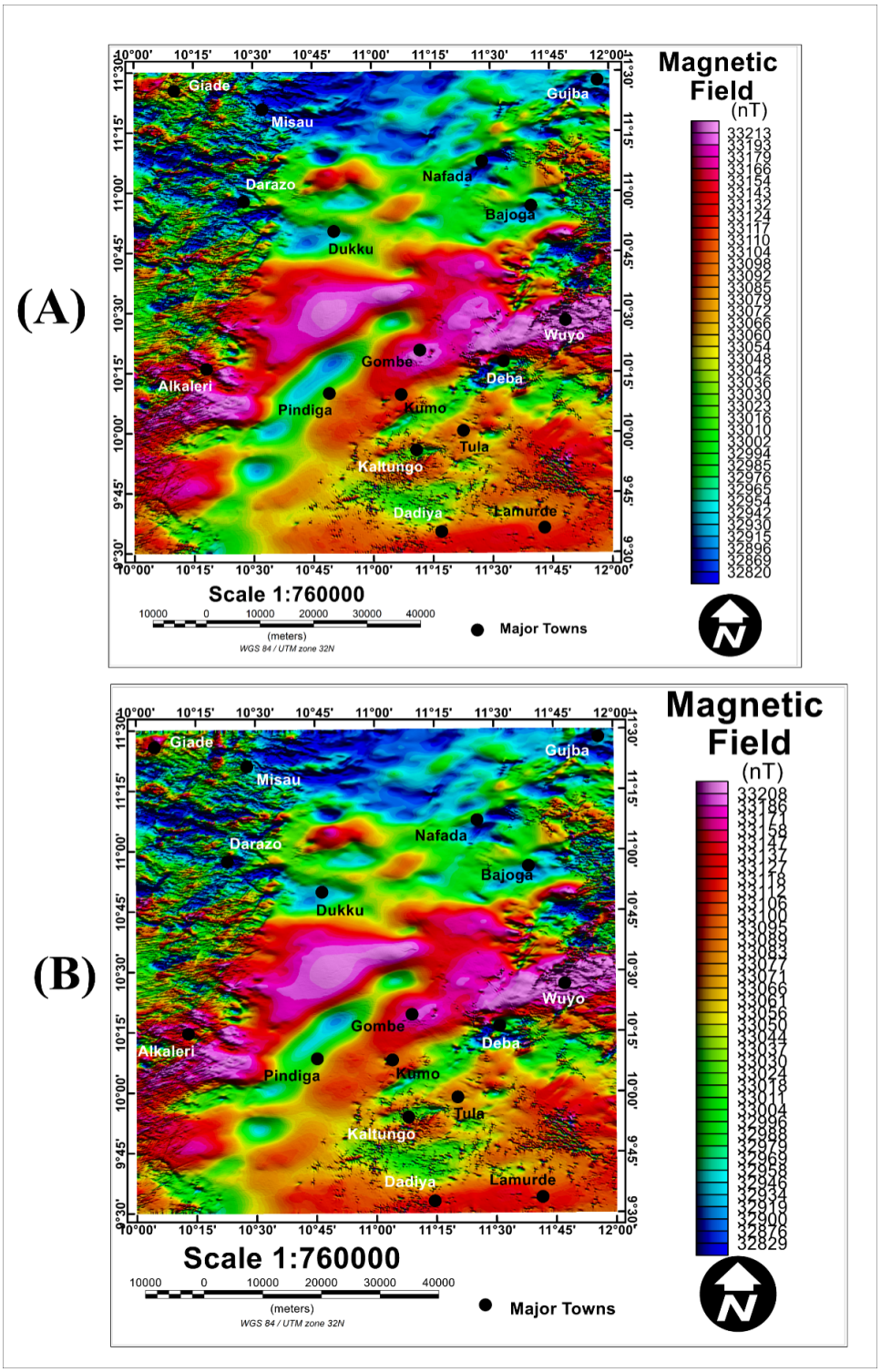

FIGURE 2. (a) Total Magnetic Field Intensity (TMI) map of the study area, and (b) Reduced to magnetic equator (RTE-TMI) map of the study area

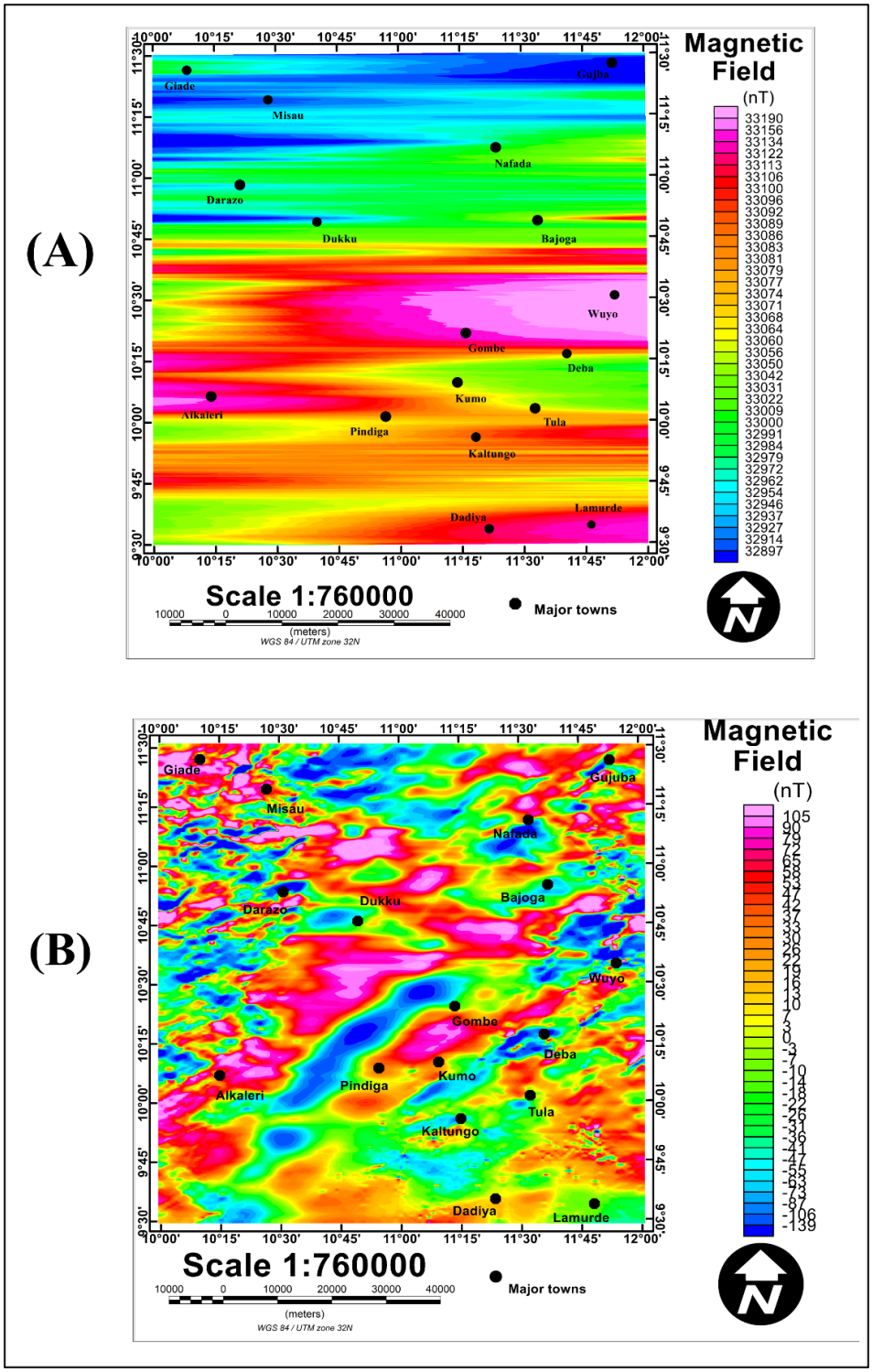

FIGURE 3. a) Regional Magnetic field map of the study area separated from the total magnetic field (RTE-TMI) map using polynomials fitting method, and (b) Residual field map of the study area

According to Nabighian (1984) and Roest et al. (1992), the analytic signal of a given magnetic anomaly can be computed by taking the square root of the total of squares of the magnetic signal derivatives along the x,

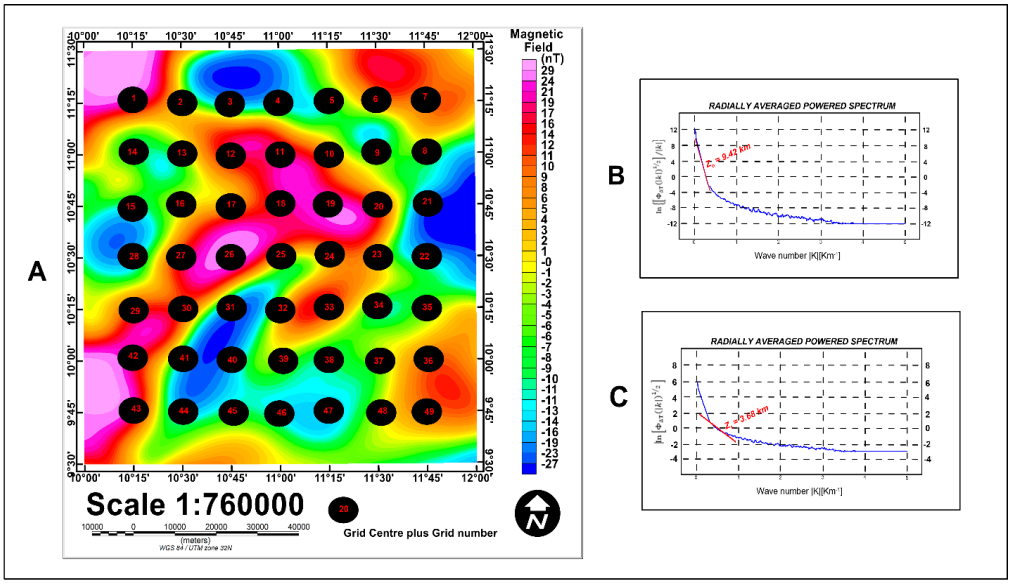

FIGURE 4. a) A 15 km upward continued residual map of the study area showing the 49 grids with its Centre denoted by square and a number, (b) and (c) Radially average powered spectrum for blocks 1-2 used for depth estimation in a slope plot program mounted on a Matlab software

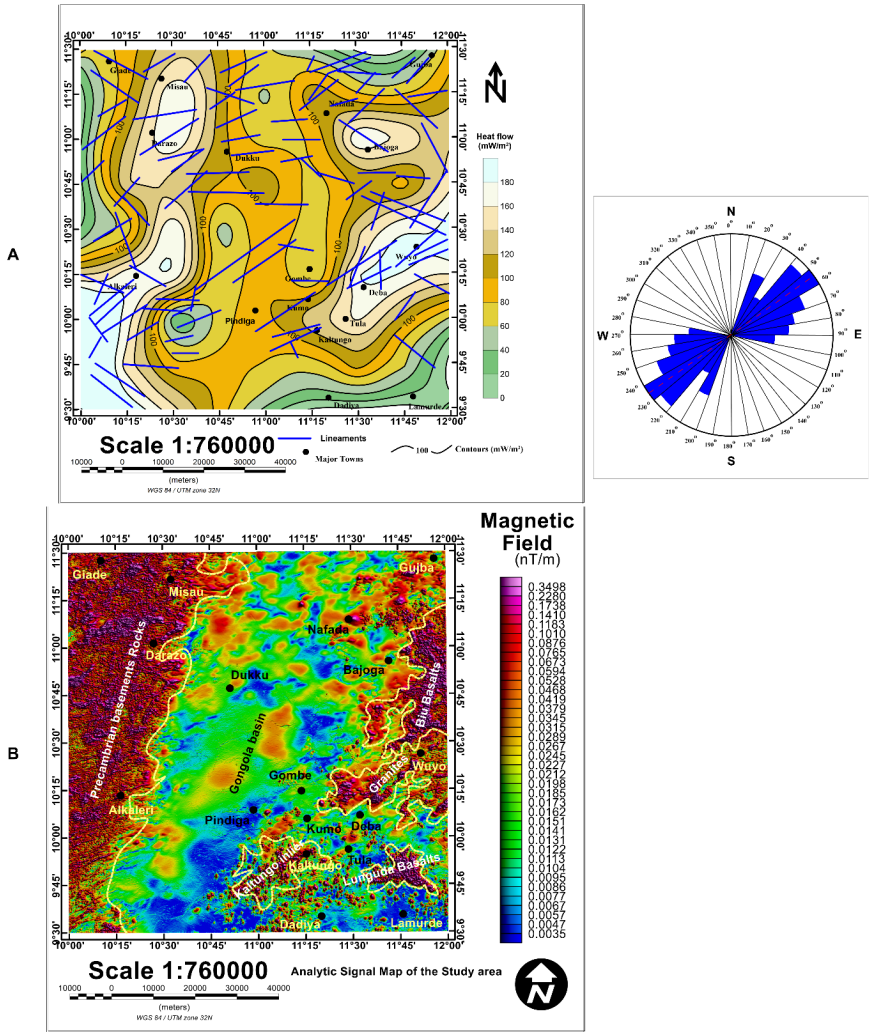

FIGURE 5. a) Magnetic lineaments overlaid on the heat flow map, and a rose plot showing the pattern of the tectonic lineaments distribution in the area, and (b) Analytic signal map of the study area showing the major rock types distribution as shown by their magnetic contrasts

y, and z directions of the field. The analytic signal filter is superior to other filters in that it is insusceptible to the IGRF field direction, which means that there is no need for preceding this filtration with a reduction to the equator filter. Therefore, the analytic signal filter was applied directly to the TMI data of the research area using the MAGMAP tool of the Oasis environment. The analytic signal map of the area helps in clearly demarcating the boundaries (contacts) of the main rock types (basement rocks outcrop, the sedimentary Gongola basin outline, Biu and Lunguda basalts, and the location of the Kaltungo Inlier) distributed in the study area from their differences in magnetic susceptibility contrast (Figure 5(b)).

There are several methods for depth to basement computations, including spectral analysis methods (Bahruddin et al. 2020), Euler deconvolution, Werner deconvolution, 2-D modelling, analytic signal depth computation, and the source parameter imaging (SPI) method. However, the use of source parameter imaging was preferred in this study because of the advantages that this method has over others. These include its non-dependence on magnetic inclination, declination, dip, strike, and remnant magnetization.

The SPI, otherwise known as the local wave number approach, was first invented by Thurston and Smith (1997). SPI involves a depth estimation using the local wave numbers of the analytic signal field of the study area. The SPI grid was calculated by inputting dx, dy, and dz as pre-processed grids obtained from the processing of the residual data (grid). The dx, dy, and dz serve as the input grids for the generation of the SPI grid for the study area. The use of lower order derivatives was ensured while calculating the input grids (dx, dy, and dz). This was configured to minimize noise, as the method is noise sensitive at higher orders (Salako 2014). The expression for the SPI depth computation is presented in the work of Thurston and Smith (1997).

TABLE 1. Computed Curie-point depths, temperature gradients, and sub-surface heat flow values

Block No.	Coordinates	Centroid Depth (Z_0), (km)	Depth to the top Sources (Z_t) (km)	Curie Point Depth (Z_b, (km)	Temperature Gradient (dT/dZ), °C/km	Heat flow (mW/m^2)
1	10°15′E, 11°15′N	9.42	3.68	15.16	38.26	95.650
2	10°30′E, 11°15′N	6.10	3.95	8.25	70.30	175.75
3	11°45′E, 11°15′N	9.37	3.77	14.97	38.74	69.730
4	11°00′E, 11°15′N	10.80	3.66	17.94	32.33	58.190
5	11°15′E, 11°15′N	6.66	3.90	9.042	64.15	110.83
6	11°30′E, 11°15′N	8.11	3.66	12.56	46.18	83.140
7	11°45′E, 11°15′N	9.68	3.36	16.00	36.25	90.630
8	11°45′E, 11°00′N	6.48	3.69	9.27	62.57	156.43
9	11°30′E, 11°00′N	6.11	3.74	8.48	68.40	171.00
10	11°15′E, 11°00′N	6.77	3.21	10.33	56.15	101.07
11	11°00′E, 11°00′N	8.76	3.54	13.98	41.49	74.680
12	10°45′E, 11°00′N	6.67	4.08	9.26	62.64	112.75
13	10°30′E, 11°00′N	6.22	4.06	8.38	69.21	173.03
14	11°15′E, 11°00′N	12.90	4.54	21.26	27.28	68.20
15	10°15′E, 10°45′N	7.39	3.90	10.88	53.31	133.28
16	10°30′E, 10°45′N	7.03	3.10	10.96	52.92	132.30
17	10°45′E, 10°45′N	6.99	3.51	10.47	55.40	99.720
18	11°00′E, 10°45′N	6.50	3.38	9.62	60.29	108.52
19	11°15′E, 10°45′N	8.76	3.61	13.91	41.71	75.080
20	11°30′E, 10°45′N	8.58	3.37	13.79	42.06	105.12

21	11˚45′E, 10˚45′N	9.13	3.21	15.05	38.54	96.350
22	11˚45′E, 10˚30′N	6.07	3.96	8.18	70.91	177.28
23	11˚30′E, 10˚30′N	7.30	3.71	10.89	53.26	133.15
24	11˚15′E, 10˚30′N	8.98	3.36	14.60	39.73	71.510
25	11˚00′E, 10˚30′N	7.21	3.51	10.91	53.16	95.690
26	10˚45′E, 10˚30′N	11.0	3.78	18.22	31.83	57.290
27	10˚30′E, 10˚30′N	6.02	3.82	8.22	70.56	176.40
28	10˚15′E, 10˚30′N	12.0	3.92	20.08	28.88	72.200
29	10˚15′E, 10˚15′N	6.30	4.11	8.49	68.32	170.80
30	10˚30′E, 10˚15′N	6.30	4.14	8.46	68.56	171.40
31	10˚45′E, 10˚15′N	10.20	3.51	16.89	34.34	61.810
32	11˚00′E, 10˚15′N	7.06	3.56	10.56	54.92	98.860
33	11˚15′E, 10˚15′N	10.3	3.60	17.0	34.12	61.410
34	11˚30′E, 10˚15′N	6.13	3.96	8.30	68.88	174.70
35	11˚45′E, 10˚15′N	6.24	4.26	8.22	70.56	176.40
36	11˚45′E, 10˚00′N	8.67	3.45	13.89	41.76	104.40
37	11˚30′E, 10˚00′N	6.39	3.80	8.98	64.59	161.48
38	11˚15′E, 10˚00′N	7.30	3.50	11.10	52.25	130.63
39	11˚00′E, 10˚00′N	8.03	3.86	12.20	47.54	118.85
40	10˚45′E, 10˚00’N	9.59	3.44	15.74	36.85	66.300
41	10˚30′E, 10˚00′N	17.5	3.52	31.48	18.42	33.150
42	10˚15′E, 10˚00′N	6.35	4.24	8.46	68.56	174.40
43	10˚15′E, 9˚45′N	6.57	3.66	9.48	61.18	152.95
44	10˚30′E, 9˚45′N	8.03	4.06	12.00	48.33	86.990
45	10˚45′E, 9˚45′N	7.76	3.62	11.90	48.74	87.730
46	11˚00′E, 9˚45′N	8.61	3.85	13.37	43.38	78.080
47	11˚15′E, 9˚45′N	9.27	3.67	14.87	39.00	70.200
48	11˚30′E, 9˚45′N	6.57	3.27	9.87	56.56	105.40
49	11˚45′E, 9˚45′N	13.6	3.35	23.85	24.32	60.80

Average CPD: 13.0 km, Average temp. Grad; 50.2 °C/km, Average heat flow; 110.65 mW/m^2

Results and Discussion

A map showing the variation of CPD over the study area is presented in Figure 6(c). Careful examination of the map shows that there are areas or regions within the study area that show moderate to high CPD anomalies (15 km to >30 km). Those areas (anomalies **H** and **L**) are located near the north-western and western parts of Gombe town, which is in turn located within the central portion of the study area. Other areas showing moderate to high (deep) CPD anomalies (**I**, **J, K**, and **M**) included Giade, Gujba, south-east of Bajoga, western Dadiya, western Pindiga, and an area near south of Darazo/north of Alkaleri town (Figure 6(c)). However, anomalies **A**, **B**, **C**, **D**, **E**, **F** and, **G**, that were located near Nafada, Bajoga, Darazo, Dukku, Alkaleri, Deba, Wuyo, Tula, and Misau showed low to very low anomalous CPD values (≤14 km) (Figure 6(c)). The minimum CPD value of 8.18 km was found at block 22 as shown in Table 1. Moreover, 31.48 km was the maximum CPD value, found at block 41, while the average CPD for the 49 blocks was 13.0 km (Table 1).

The shallow (low-very low) CPDs (8.18 km to 14 km) calculated from the present study shows relative conformity with the findings of Obande et al. (2014), whose study around Wikki warm spring, Nigeria, using lower resolution airborne magnetic data, reported very

shallow CPDs that range from 6 km - 12 km, with an average of 8 km. Moreover, Mono et al. (2018), whose study was also conducted within the African continental part of Cameroun also reported shallow CPDs (5.22 -14.35 km) around Loum - Minta areas, with an average of 9.09 km.

Areas of shallow CPDs (corresponding to high heat flow and high temperature gradient zones) found near the Alkaleri, Wuyo, Misau, Tula, Nafada, Bajoga, and Darazo areas are in accordance with the findings of Abdullahi et al. (2014); these findings reported the manifestation of local geothermal activities such as the occurrence of numerous volcanic plugs and Pan-African granitic intrusions around the same Alkaleri (basement complex) area, Billiri-Kaltungo areas, and the exposures of tertiary basalts at the Biu and Lunguda Plateaus.

Moreover, the display of shallow CPDs/high heat flow/high temperature gradients around the eastern parts (Nafada/Bajoga areas) provides a possible explanation to the previous report by NESREA (2011). This report stated that emissions of harmful and environmentally hazardous gases occurred for approximately 7 months from a previously dormant volcanic intrusion located within the Pindiga formation of the study area, near Abaduguri village. Furthermore, the locations of some fumaroles (Wikki warm spring) near the basement areas (Alkaleri areas) at the western part of study area as well as the location of the Ruwan-Zafi warm spring around the Lamurde anticlinal area, as reported by Kurowska and Schoenich (2010) and Abdullahi et al. (2014), showed relative conformity with the areas of moderate-high heat flow/moderate-shallow CPDs presented in this study.

From a visual observation of the depth to magnetic basement map (Figure 6(a)) generated for the study area, using the SPI approach, areas displaying shallow, moderate, and deep depth to basement (thicknesses of sediments) values can be observed. These depths (shallow, moderate, and deep parts) are represented by reddish to magenta, greenish to yellowish, and light to dark blue coloured anomalies, respectively. Areas depicting the greatest (deepest) depth to basement configuration (3.055 km) within the study area are located around western parts of Gombe, Pindiga, Dukku, Nafada, Bajoga, and the eastern parts of Alkaleri town. The areas with the deepest as well as moderate depth to basement values are situated within the Gongola basin, while areas with the shallowest depth to basement (0.610-0.802 km) occupied the eastern and western parts of the study area. These include areas around Misau, Giade, Darazo, Alkaleri, Kaltungo, Tula, Dadiya, Lamurde, Deba, and Wuyo towns. These areas are dominated by surface or near surface exposures of basement/volcanic rocks as showed by NGSA (2009) (Figure 1(b)).

The deepest depth to basement zones found within the study area, especially in locations around Gombe, Pindiga, and Nafada, show a degree of conformity with the findings of Salako and Udensi (2013) and Salako (2014), who also used an older (1974-1980) and lower resolution aeromagnetic data to calculate the depth of the basement configuration. Their studies also reported shallow depths around western parts (basement outcropped area), the Kaltungo inlier, and Wuyo (Biu basalt outcrops).

Furthermore, a visual observation and comparison of both the CPD map (Figure 6(c)) and inverted depth to magnetic basement map over the study area (Figure 6(a)) showed overlaps of some zones with the deepest CPD values with those having the thickest sedimentary piles (deepest depth to basement). These overlaps can be found around the western parts of Gombe, as well as the Dukku, Bajoga, and eastern Alkaleri areas. Careful examinations of the analytic signal map (Figure 5(b)), CPD map (Figure 6(c)), and the depth to magnetic basement map of the study area (Figure 6(a)) shows that some of these low magnetic susceptibility zones (sedimentary rock outcrops) have a deep CPD as well as the deepest depth to magnetic basement; this could be as a result of crustal thinning processes that occurred within the formation process of the Benue trough during the Jurassic period (Guiraud 1993). However, other areas with shallow CPDs and high magnetic susceptibility contrasts (from the analytic signal map) as well as shallow depth to magnetic basements resulted from magmatic intrusions that characterized many parts of the Benue trough of Nigeria (Osazuwa et al. 1981).

The temperature gradient for each of the 49 spectral blocks was calculated using the following equation: $\frac{\partial t}{\partial Z} = \left(\frac{\theta}{Z_b}\right)$. A map showing the variation of the temperature gradient is shown in Figure 6(d). Table 1 presents the values of the temperature gradient for each of the previously mentioned blocks. The minimum value of the temperature gradients was recorded at block 41, at 18.42 °C/km, whereas the maximum temperature gradients were obtained at block 22 of the study area, at 70.91 °C/km. Moreover, the average temperature gradient of the study area was 50.2 °C/km. An observation of the temperature gradient map generated and presented in Figure 6(d) shows areas that are characterized by moderate to high values (51 °C/km to ≥ 70 °C/km); these include anomalies **A**, **B**, **C**, **D**, **G**, and **F** found near

Darazo, Bajoga, Dukku, Alkaleri, Wuyo, Deba, parts of Misau, Tula, as well as anomaly **E**, located northwest of Nafada town. However, other anomalies (**H**, **I, J, K, L, M,** and **P**) portray low to very low temperature gradients (≤ 50 °C/km) and are found at the central areas of the map (Gombe and Bajoga areas), extreme north western areas (Giade), extreme northeast locations (Gujba) and extreme southeastern parts of the map (Dadiya and Lamurde). A study by Nwankwo et al. (2009), which used bottom hole temperature measurements from the genetically related neighbouring Bornu basin, reported temperature gradients ranging from 30 °C/km to 40 °C/km, with an average of 34 °C/Km, which is lower than the average of 50.2 °C/km within the present study. Moreover, the geothermal study by Kurowska and Schoenich (2010) presented temperature gradients ranging from 11 °C/km to 59 °C/km, which were obtained from bottom hole temperature (BHT) measurements of oil wells of the adjacent Bornu basin. The temperature gradient range of 18.42 °C/km - 70.91 °C/km from the current study is comparatively higher than the range within the study by Kurowska and Schoenich (2010). The higher temperature gradients recorded compared to the bottom hole temperature studies could be attributed to the non-extensiveness (localization) of the data coverage associated with those studies, compared to the present more extensive airborne magnetic data usage approach, this tends to give a broader view of the thermal constituents of the area. Moreover, the present results (with an average of 50.2 °C/km) when compared with results obtained by Obande et al. 2014 (with an average of 68 °C/km) using older (1974) and lower resolution aeromagnetic data around Wikki warm spring area shows that results gotten from both studies have higher temperature gradients than the previously mentioned bottom hole temperature studies, due to the coverage advantage of the latter over the former. The study by Mono et al. (2018) using airborne magnetic data around the neighbouring Cameroonian terrain also show higher average temperature gradients of 72.24 °C/km.

The amount of heat flow over the study area was derived using the equation: $Q = \lambda\left(\frac{\theta}{Z_b}\right)$, and the heat flow values for each spectral block were computed and presented in Table 1. The minimum heat flow value of the study area was 33.15 mW/m^2 in Block-41, which was lower than the minimum value of 63.6 mW/m^2 reported by Nwankwo et al. (2009) from BHT measurements obtained from the adjacent Bornu basin. However, the maximum value of 105.6 mW/m^2 of heat flow from the Bornu basin as reported by the authors was slightly lower than the maximum value of 177.28 mW/m^2 (Block-22) (Table 1) obtained from the genetically related Gongola basin (present study). The average heat flow over the research area was 110.65 mW/m^2 (Table 1), which was greater than the average heat flow value of 80.6 mW/m^2 reported by Nwankwo et al. (2009). Figure 6(e) provides information concerning the variation of heat flow over the study area. Careful observation of this map shows areas depicting higher, lower, and moderate values of heat flow. Areas around Darazo, Misau, and Dukku (all in the north-western part of the map) shows moderate to high heat flow anomalies (**A** & **B**). Moreover, areas towards the eastern Nafada and northern parts of Bajoga town (in the northeastern part of the study area) displays moderate to high heat flow anomaly (**C**) (Figure 6(e)). Other areas showing moderate to high values of heat flow anomalies (**D** & **E**) are Wuyo, Deba, Tula, Alkaleri, and an area near the south-western part of Pindiga town. Areas displaying low to very low heat flow anomalies found at the central, extreme northwest, extreme northeast, and extreme south-eastern parts of the study area are represented by anomalies **G**, **H**, **I**, **J**, **K**, **L**, and **M** (Figure 6(e)).

According to Ross et al. (2006), the variation in CPD over a given area is related to the geology of the area. CPD values show obvious decreases over volcanic and tectonically active zones globally, at 15-25 km along island arc/ridges and greater than 30 km along trenches (Ross et al. 2006). An examination of the areas of anomalous occurrences of CPD (areas with very low to low CPD) when overlaid with the geology of the study area (Figure 7(a)) showed that some of the areas with the shallowest CPD were either on or close to crystalline basements/volcanic geological terrain or other tectonic lineament zones (regional faults, fractures). The shallow nature of the CPD around these zones could be attributed to the high heat conductivity of those terrains as well as the presence of magmatic intrusions (plutons) below them (Mono et al. 2018). This can be supported by the possession of greater magnetization contrasts along the shallow CPD anomalies in the analytic signal map as overlaid on the CPD contour map presented in Figure 7(b). For example, anomalies around Wuyo, Alkaleri, and parts of Misau were overlain either completely or partly on the older Basalts, banded gneiss/charnokytes/Keri-Keri Formation, and med-coarse grained biotite-biotite hornblende gneiss/Keri-Keri Formation, respectively. Some locations depicting moderate to high geothermal gradients as well as high heat flow corresponded to shallow CPD values. However, the map also showed

that some areas had moderate to deep CPD anomalies that corresponded to locations found mostly within the sedimentary outcrops of Keri-Keri, Gombe, and Pindiga Formations of the Gongola basin. These areas include an area due west of Gombe, as well as the Bajoga, Pindiga, Dadiya, and Lamurde areas (Figure 7(a)); they display a small magnetization contrast as displayed in the analytic signal map. These areas can be attributed to the thick sedimentation below them. The thick sedimentary piles were derived from the source parameter imaging method (Figure 6(a)).

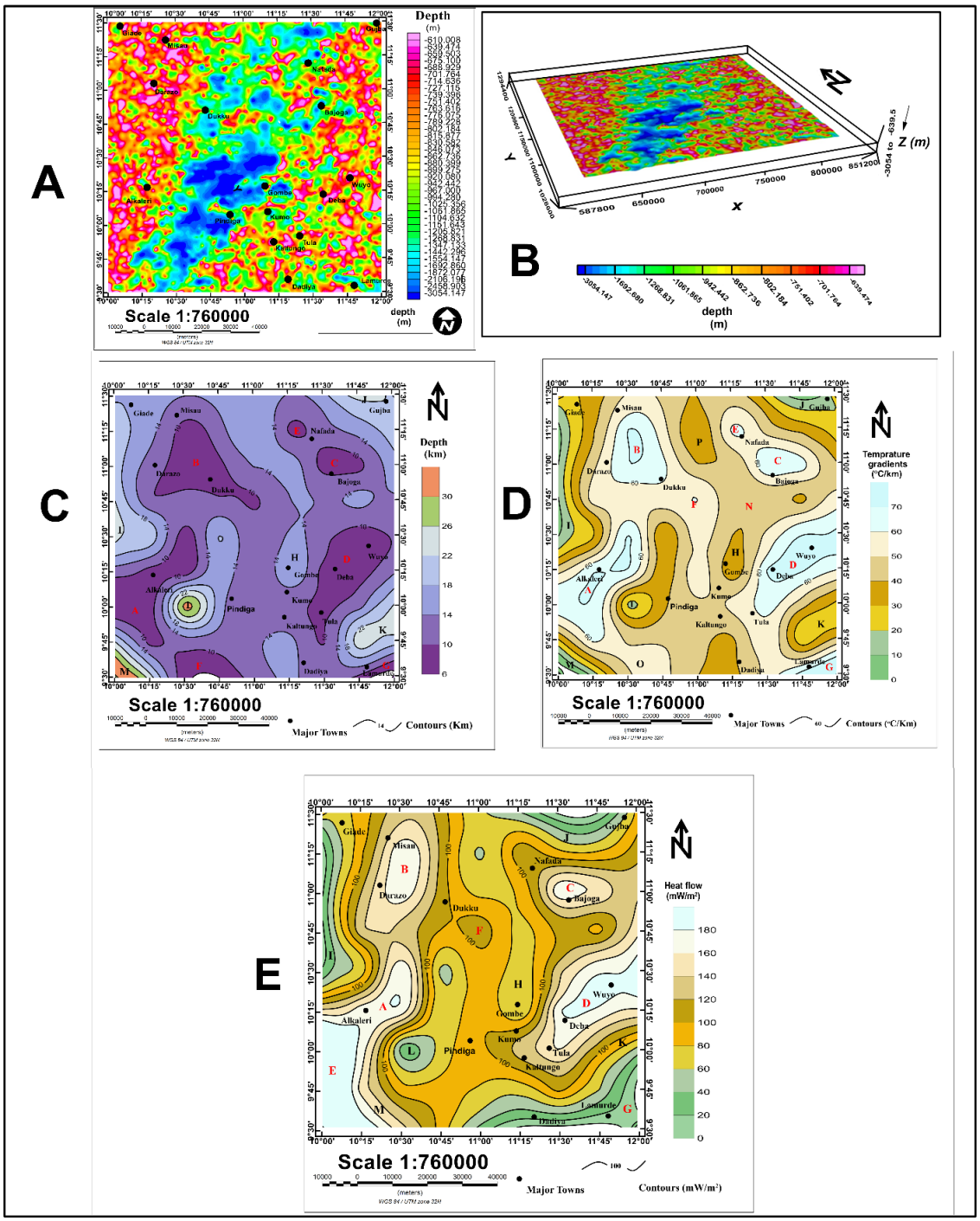

FIGURE 6. a) Source parameter imaging (SPI) map showing magnetic basement depth/ basement configuration of the study area, (b) Three-dimensional view of source parameter Imaging (SPI) map of the study area showing inverted depth to magnetic basement, (c) Curie-point depth (CPD) map of the study area, (d) Temperature gradient map of the research area, and (e) Heat flow map of the study area

Most of the areas depicting moderate to high temperature gradients anomalies correlate either completely or partly with the crystalline basement/ Volcanic rocks of the geologic map of the study area. For example, anomalous areas around Alkaleri (correlates with Migmatite-gness, Banded-gneiss, and parts of Keri-Keri Formation), parts of Darazo (correlates with exposures of Biotites-biotites hornblende granites, Ignimbrites, and parts of Keri-Keri Formation), Wuyo (Older basalts, banded gneiss, medium-coarse grained biotite - biotite hornblende granites, porphyritic biotite - biotite hornblende granites), an east of Nafada area, Deba (Bima Formation) and parts of Tula showed their relative correlation either completely or partially with their crystalline basement/volcanic geology (Figure 8(a)). However, greater parts of the areas showing low to very low temperature gradients corresponds to less conductive sedimentary outcrops of Pindiga, Gombe, and parts of Keri-Keri Formations of the Gongola basin (Figure 8(a)).

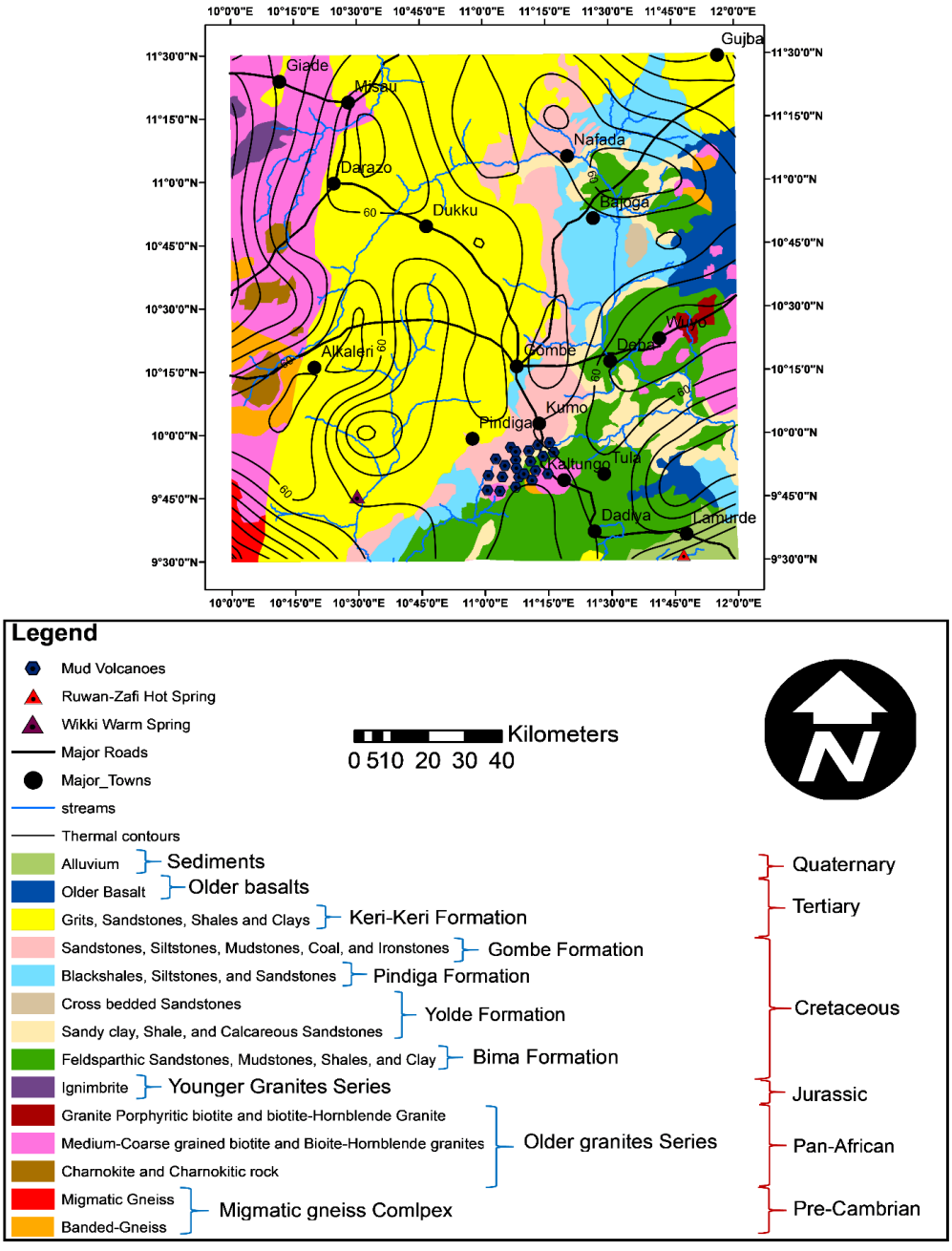

FIGURE 7. a) Curie-point depth contour map overlaid on the geologic map of the study area (Contour Interval; 1 km)

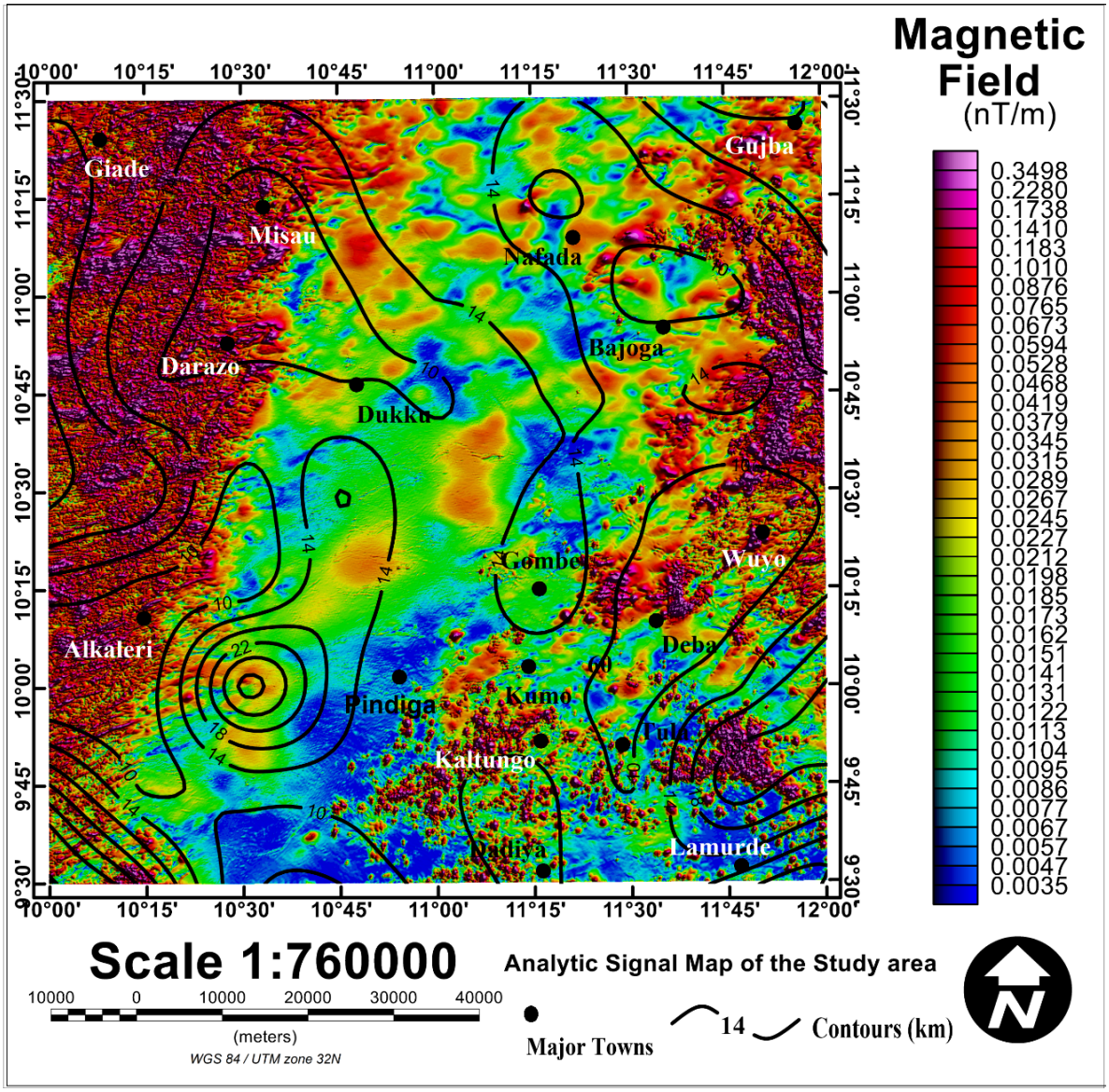

FIGURE 7. b) Curie-point depth (CPD) map overlaid on the analytic signal map of the study area showing relationship between areas of different magnetization contrast with their CPDs

Locations of the heat flow, and temperature gradients maps showing high values corresponds to regions depicting shallow CPD. Therefore, this can be attributed to the occurrence of shallow depth to interface between brittle to plastic deformation within the crustal regions around. It could also be due to magmatic intrusions (Dolmaz et al. 2005). These also corresponds to those geological terrains that have high thermal conductivity (volcanic/basements) and tectonic lineaments zones (Figure 5(a)), that includes; Wuyo (older basalts, banded gneiss, medium-coarse grained biotite - biotite hornblende granites, porphyritic biotite - biotite hornblende granites), Alkaleri (Migmatites - gneiss, Banded-gneiss, and parts of Keri-Keri Formation), eastern parts of Nafada, Parts of Darazo, and Misau towns. Likewise, regions with high Curie point depths coincides with the low geothermal gradients/low heat flow. Moreover, terrains with low to very low heat conductivity that coincides with thick sedimentary piles includes; Pindiga, Gombe, and parts of Keri-Keri Formations (Figure 8(b)). The high heat flow/ high geothermal gradients anomalies having values

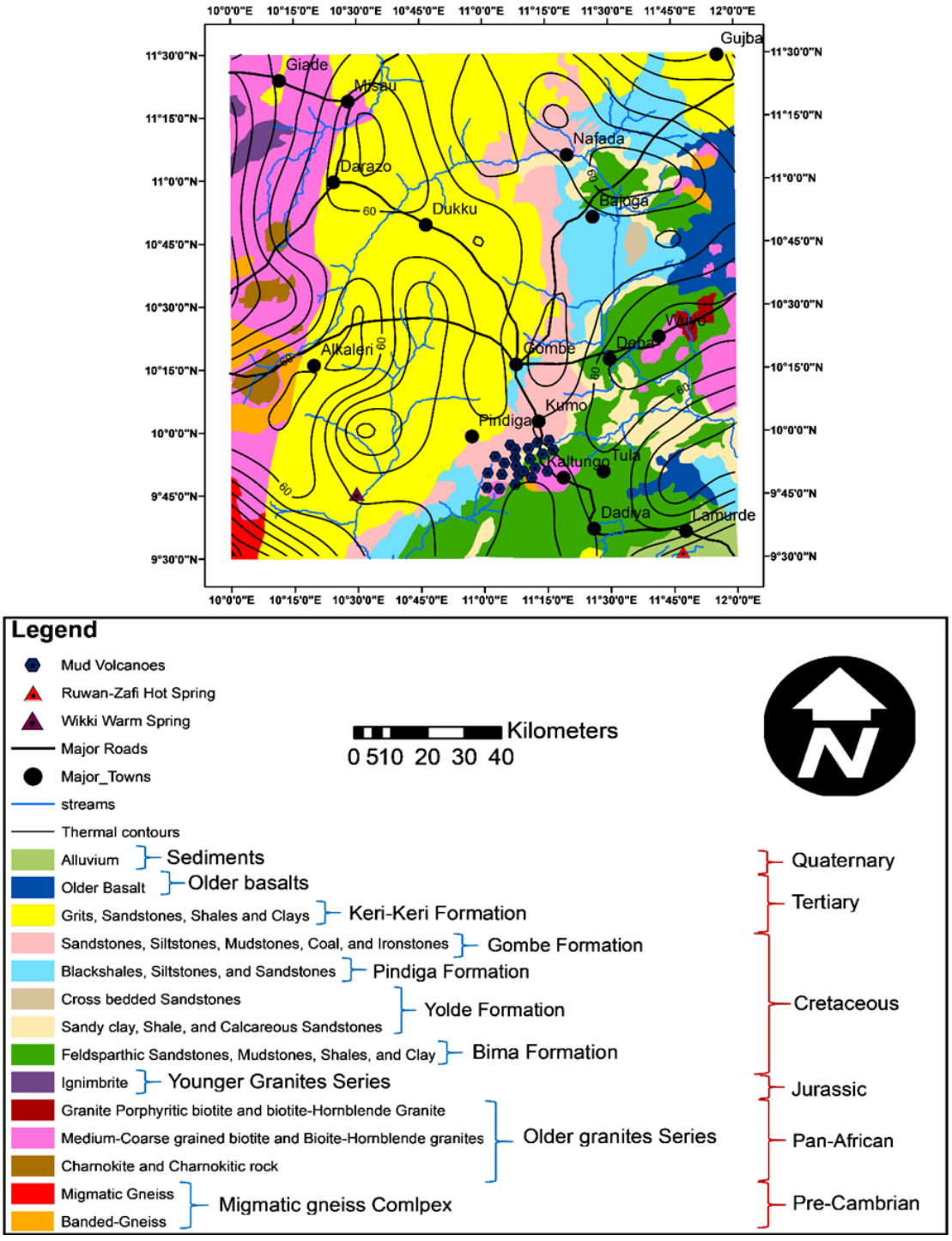

FIGURE 8. a) Temperature gradients contour map overlaid on the geologic map of the study area (Contour intervals; 1 °C/km)

greater than 60 mW/m^2 (Mono et al. 2018) which is the average heat conductivity of a normal continental crust are considered to be high, and as such are abnormal. Therefore, heat flow values greater than 80-100 mW/m^2 shows abnormal situations (Jessop et al. 1976). Now, the regions of the study area showing shallow CPDs/ high temperature gradients/high heat flow are attributed to crustal thinning, magmatic up-welling, as well as

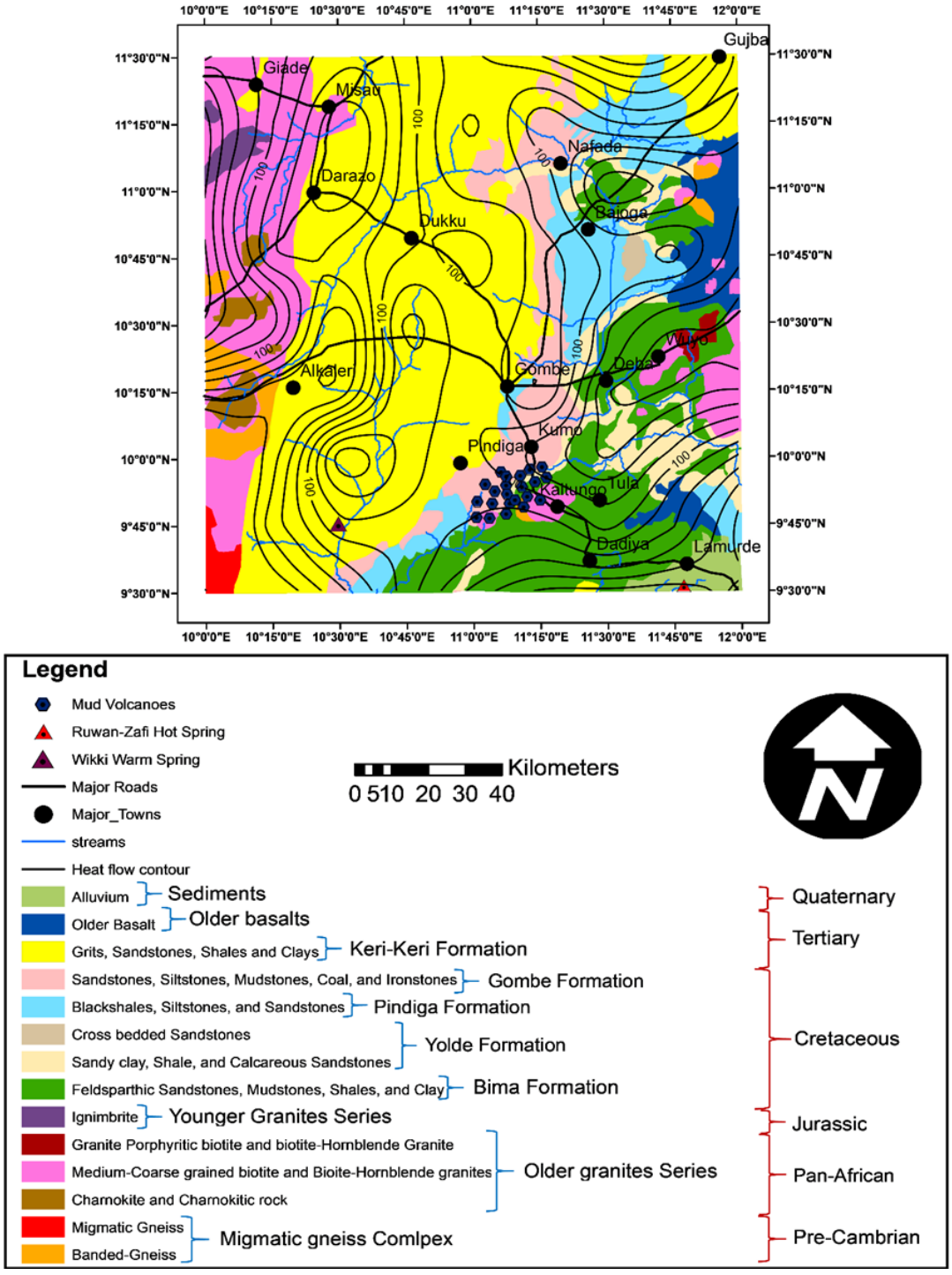

FIGURE 8. b) Heat flow map of the study area overlaid on the geologic map of the study area (Contour Intervals; 1 mW/m^2)

fracturing and faulting processes that occurred during formation process of the Benue trough during the Jurassic times (Nwajide 2013; Obaje 2009). Moreover, the rose plot pattern of the magnetic lineaments (Figure 5(a)) shows a dominant trend in the NE-SW direction. This conforms to the regional trend of Benue trough as showed by the findings of Abdullahi et al. (2019).

Conclusion

The spectral analysis method was used to analyse aeromagnetic data collected over the entire Gongola basin and its environs in Nigeria. This approach was used to determine the geothermal implications of the study area through estimating the CPD, the temperature gradients, and subsurface heat flow. The estimated CPDs ranges from: 8.18 km to 31.48 km. The shallowest CPD anomalies were found within the Alkaleri, Darazo, Misau, Wuyo, eastern Nafada/Bajoga, and Deba areas. They are located along basements, volcanic, and sedimentary rock outcrops characterized by the presence of regional faulting. Moderate to high CPDs anomalies (15 - 31.48 km depth) were identified around the central parts of the study area (near the western and eastern parts of Gombe town). The areas with the greatest CPDs (depth >30 km) found around the western part of Gombe and Pindiga towns coincides with the sedimentary rock units of the study area. The computed geothermal gradients ranges from 18.42 °C/km to 70.91 °C/km, respectively. Whereas, the estimated heat flow for the entire Gongola basin and its environs ranged from 33.15 mW/m^2 to 177.28 mW/m^2. Thus, areas of high heat flow, high geothermal gradients as well as shallow CPDs are considered as new promising targets for future geothermal exploration.

Overall, the areas displaying the shallowest CPDs can be attributed to crustal thinning and intrusions of younger magmatic events, whereas regions with deeper CPDs are attributed to the presence of thick crusts or crustal thickening.

Acknowledgements

The authors wish to express their gratitude to the School of Physics, Universiti Sains Malaysia, for providing us with the various software used for the processing of the magnetic data. We also acknowledged the financial support rendered by the 'Tertiary Education Trust Fund (TETFund)', and 'RUI Grant, Burning in the Southeast Asian Maritime Continent: Solving Smoke Direct and Semi-Direct Radiative forcing through: AeroNet and MPLNET constraints, 1001/PFIZK/8011079', to Principal author of this research. Special appreciation goes to Nigerian Geological Survey Agency (NGSA) for the release of the aeromagnetic data used for the present research. The authors of the present work expressed no conflict of interest of any kind.

References

Abdullahi, B.U., Rai, J.K., Olaitan, O.M. & Musa, Y.A. 2014. A review of the correlation between geology and geothermal energy in Northeastern Nigeria. *IOSR Journal of Applied Geology and Geophysics (IOSR-JAGG)* 2(3): 74-83.

Abdullahi, M., Singh, U.K. & Roshan, R. 2019. Mapping magnetic lineaments and subsurface basement beneath parts of Lower Benue Trough (LBT), Nigeria: Insights from integrating gravity, magnetic and geologic data. *Journal of Earth System Science* 128(1): 17.

Abraham, E., Itumoh, O., Chukwu, C. & Rocks, O. 2019. Geothermal energy reconnaissance of Southeastern Nigeria from analysis of aeromagnetic and gravity data. *Journal of Pure and Applied Geophysics* 176: 1615-1638.

Abdel Zaher, M., Saibi, H., Mansour, K., Khalil, A. & Soliman, M. 2017. Geothermal exploration using airborne gravity and magnetic data at Siwa Oasis, Western Desert, Egypt. *Renewable and Sustainable Energy Review* 83(Part 2): 3824-3832. http://dx.doi.org/10.1016/j.rser.2017.10.088.

Adepelumi, A.A. & Falade, A.H. 2017. Combined high-resolution aeromagnetic and Radiometric Mapping of uranium mineralization and tectonic settings in Northeastern. *Acta Geophys.* 65: 1043-1068.

Aboud, E., Salem, A. & Mekkawi, M. 2011. Curie depth map for Sinai Peninsula, Egypt Deduced from the analysis of magnetic data. *Tectonophysics* 506: 46-54.

Abubakar, M.B. 2006. Biostratigraphy, Palaeo environment and organic geochemistry of the Cretaceous sequences of the Gongola Basin, Upper Benue Trough, Nigeria. PhD. Thesis, Abubakar Tafawa Balewa University, Bauchi, Nigeria (Unpublished). pp. 139-140.

Ajayi, C.O. & Ajakaiye, D.E. 1981. The origin and peculiarities of the Nigerian Benue Trough: Another look from the recent gravity data obtained from the middle Benue. *Tectonophysics* 80: 285-303.

Bahruddin, N.F.D., Hamza, U. & Jacob, W.Z.W. 2020. Estimation of Earth Structure by satellite gravity analysis of Peninsular Malaysia. *Sains Malaysiana* 49(7): 1509-1520. http://dx.doi.org/10.17576/jsm-2020-4907-04.

Baioumy, H., Nawawi, M., Wagner, K. & Arifin, M.H. 2014. Geochemistry and geothermometry of non-volcanic hot springs in West Malaysia. *Journal of Volcanology and Geothermal Research* 290: 12-22.

Bello, R., Ofoha, C. & Wehiuzo, N. 2017. Geothermal gradient, Curie point depth and heat flow determination of some parts of lower Benue trough and Anambra basin, Nigeria, using high resolution aeromagnetic data. *Phys. Sci. Int. Journal* 15(2): 1-11.

Billim, F., Akay, T., Aydemir, A. & Kosaroglu, S. 2015. Curie point depth, heat-flow and radiogenic heats production deduced from spectral analysis of the aeromagnetic data for investigation on the Menderes Massif and the Aegean Region, western Turkey. *Geothermic* 60: 44-57.

Blakely, R.J. 1995. *Potential Theory in Gravity and Magnetic Applications.* Cambridge: Cambridge University Press.

Correa, R.T., Vidotti, R.M. & Oksum, E. 2016. Curie surface of Borborema Province, Brazil. *Tectonophysics* 679: 73-87.

Cordell, L. & Grauch, V.J.S. 1985. Mapping basement magnetization zones from aeromagnetic data in the San Juan Basin, New Mexico, In *The Utility of Regional Gravity and Magnetic Anomaly Maps*, edited by Hinze, W.J. pp. 181-197.

Dentith, M. 2011. Magnetic methods, airborne. In *Encyclopedia of Solid Earth Geophysics*, vol 1, edited by Gupta, H.S. Springer, Dordrecht. pp. 761-766.

Dolmaz, M.N., Ustaomer, T., Histarli, Z.M. & Orbay, N. 2005. Curie point depth variations to infer Thermal Structure of the crust at the African-Urasian convergence zone, SW Turkey. *Earth Planets Space* 57: 373-383.

Dunlop, D.J. & Ozdemir, O. 2001. Beyond Neel's Theories: Thermal demagnetization of a narrow-band partial thermoremnent magnetizations. *Physics of the Earth and Planetary Interiors* 126: 43-57.

Elbarbary, S., Abdel Zaher, M., Mesbah, H., El-Shahat, A. & Embaby, A. 2018. Curie point depth, Heat flow and geothermal gradients maps of Egypt deduced from aeromagnetic data. *Renewable and Sustainable Energy Reviews* 91: 620-629.

Gailer, L.S., Lenat, J.F. & Blakely, R.J. 2016. Depth to Curie temperature or bottom of the magnetic sources in the volcanic zone of la Réunion hot spot. *Journal of Volcanology and Geothermal Research* 324: 169-178.

Guo, Q. & Wang, Y. 2012. Geochemistry of hot springs in the Tenchong hydrothermal areas, Southwestern China. *Journal of Volcanology and Geothermal Research* 215-216: 61-73.

Guiraud, M. 1993. Late Jurassic Rifting-Early Cretaceous Rifting and Late Cretaceous Transgressional inversion in the Upper Benue Basin (NE Nigeria). *Bulletin Centres Recherché Exploration-Production Elf-Aquitaine* 17: 371-383.

Hamidu, I. 2012. The Campanian to Maastrichtian Stratigraphic Succession in the Cretaceous Gongola Basin of North-Eastern Nigeria. Published Ph.D. Thesis, Ahmadu Bello University, Zaria (Unpublished). pp. 41-177.

Jain, S. 1988. Total magnetic field reduction-The pole or equator? A model study. *Canadian Journal of Exploration Geophysics* 24(2): 185-192.

Jessop, A.M., Hobert, M.A. & Sclater, J.G. 1976. The World heat flow data collection 1975, Geothermal Services of Canada. *Geothermal Service* 50: 55-77.

Kurowska, E. & Schoeneich, K. 2010. Geothermal Exploration in Nigeria. *Proceedings of World Geothermal Congress-2010*, Bali, Indonesia, 25-29th April, 2010.

Lowrie, W. 2007. *Fundamentals of Geophysics*. 2nd ed. Cambridge: Cambridge University Press. pp. 1-381.

Mono, J.A., Ndougsa-Mbarga, T., Tarek, Y., Ngoh, D.J. & Amougou, O.U.I.O. 2018. Estimation of Curie point depths, geothermal gradients and near-surface heat flow from spectral analysis of aeromagnetic data in the Loum - Minta area (Centre-East Cameroon). *Egyptian Journal of Petroleum* 27: 1291-1299.

Mohamed, H.S., Abdel Zaher, M., Senosy, M.M., Saibi, H., El Nouby, M. & Fairhead, D. 2015. Correlation of aero gravity and BHT data to develop a geothermal gradient map of northern western desert of Egypt using an artificial neural network. *Journal of Pure and Applied Geophysics* 172(6): 1585-1597.

Musa, O.K. 2015. Mud volcanoes on the dry land of Nigeria. PhD Dissertation. Submitted to Postgraduate School, Ahmadu Bello University Zaria, Nigeria (Unpublished).

Manea, M. & Manea, V.C. 2011. Curie point depth estimates and correlation with subduction in Mexico. *Pure and Applied Geophysics* 168: 1489. https://doi.org/10.1007/s00024-0100238-2.

Maden, N. 2010. Curie-point depth from spectral analysis of magnetic data in Erciyes Stratovolcano (Central Turkey). *Pure Applied Geophysics* 167(3): 349-358.

Nigerian Geological Survey Agency (NGSA). 2009. Geological map sheets. Nigerian Geological Survey Agency, Abuja, Nigeria. pp. 107-174.

Nwankwo, C.N. & Ekine, A.S. 2009. Geothermal gradients in the Chad Basin, Nigeria, from bottom hole temperature logs. *International Journal of Physical Sciences* 4(12): 777-783.

Nwajide, C.S. 2013. *Geology of Nigeria's Sedimentary Basins*. Lagos, Nigeria: CSS Bookshops Ltd. p. 565.

NESREA, 2011. Annual report on hazardous geological activities in Nigeria. p. 256.

Nabighian, M.N. 1984. Toward a three-dimensional-automatic interpretation of potential field data via hilbert transforms - Fundamental relations. *Geophysics* 49: 780-786.

Nagata, T. 1961. *Rock Magnetism*. Tokyo, Japan: Maruzen Company Limited. p. 350.

Obande, G.E., Lawal, K.M. & Ahmed, L.A. 2014. Spectral analysis of aeromagnetic data for geothermal investigation of Wikki Warm Spring north-east Nigeria. *Geothermic* 50: 85-90.

Obaje, N.G. 2009. *Geology and Mineral Resources of Nigeria*. Dordtecht Heidelberg London: Springer. p. 218.

Onuoha, K.M. & Ekine, A.S. 1999. Subsurface temperature variation and heat flow in the Anambra Basin, Nigeria. *Journal of African Earth Sciences* 28(3): 641-652.

Okubo, Y., Graf, R.J., Hansen, R.O., Ogawa, K. & Tsu, H. 1985. Curie point depths of the island of Kyushu and surrounding area Japan. *Geophysics* 50(3): 481-489.

Osazuwa, I.B., Ajakaiye, D.E. & Verheijen, P.J.T. 1981. Analysis of the structure of part of the upper Benue rift valley on the basis of new geophysical data. *Earth Evolution Sciences* 2: 126-133.

Ross, H.E., Blakely, R.J. & Zoback, M.D. 2006. Testing the Curie point depth in California. *Geophysics* 71(5): 151-159.

Roest, W.R., Verhoef, J. & Pilkington, M. 1992. Magnetic interpretation using the 3-D analytic signal. *Geophysics* 57(1): 116-125. doi: 10.1190/1.1443174.

Saada, S.A. 2016. Curie point depth and heat flow from spectral analysis of aeromagnetic data over the Northern part of Western Desert, Egypt. *Journal of Applied Geophysics* 134: 11-100.

Saibi, H., Aboud, E. & Gottsman, J. 2015. Curie point depth from spectral analysis of aeromagnetic data for geothermal reconnaissance in Afghanistan. *Journal of African Earth Sciences* 111: 92-99.

Saleh, S., Salk, M. & Pamukcu, O. 2013. Estimating Curie point depth and heat flow map for Northern Red Sea rift of Egypt and its surroundings, from aeromagnetic data. *Pure and Applied Geophysics* 170: 85-863.

Salako, K.A. 2014. Depth to basement determination using Source Parameter Imaging (SPI) of aeromagnetic data: An application to Upper Benue Trough and Borno Basin, Northeast, Nigeria. *Academic Research International* 5(3).

Salako, K.A. & Udensi, E.E. 2013. Spectral depth analysis of parts of Benue Trough and Borno Basin, northeast Nigeria, using Aeromagnetic data. *International Journal of Science and Research* 2(8): 48-55.

Stacey, F.D. 1977. *Physics of the Earth*. 2nd ed. New York: John Wiley and Sons. p. 414.

Tukur, A., Samaila, N.K., Grimes, S.T., Kariya, I.I. & Chaanda, M.S. 2015. Two members sub-division of the Bima Sandstone, Upper Benue Trough: Based on sedimentological data. *Journal of African Earth Sciences* 104: 140-158.

Tanaka, A., Okubo, Y. & Matsubayashi, O. 1999. Curie point depth based on spectrum analysis of magnetic anomaly data in East and Southeast Asia. *Tectonophysics* 306: 461-470.

Thurston, J.B. & Smith, R.S. 1997. Automatic conversion of magnetic data to depth, dip, and susceptibility contrast using the SPITM method. *Geophysics* 62: 807.

Verduzco, B., Fairhead, J.D., Green, C.M. & Mackenzie, C. 2004. New insights into magnetic derivatives for structural mapping. *The Leading Edge* 23(2): 116-119.

Wang, J. & Li, C.F. 2018. Curie point depths in Northeast China and their geothermal implications for the Song Liao Basin. *Journal of Asian Earth Sciences* 163: 177-193.

*Corresponding author; email: hslim@usm.my